

Coherent open-loop optimal control of light-harvesting dynamics

Filippo Caruso,¹ Simone Montangero,² Tommaso Calarco,² Susana F. Huelga,¹ and Martin B. Plenio¹

¹*Institut für Theoretische Physik, Universität Ulm, Albert-Einstein-Allee 11, D-89069 Ulm, Germany*

²*Institut für Quanteninformationsverarbeitung, Universität Ulm, Albert-Einstein-Allee 11, D-89069 Ulm, Germany*

We apply theoretically open-loop quantum optimal control techniques to provide methods for the verification of various quantum coherent transport mechanisms in natural and artificial light-harvesting complexes under realistic experimental constraints. We demonstrate that optimally shaped laser pulses allow to faithfully prepare the photosystem in specified initial states (such as localized excitation or coherent superposition, i.e. propagating and non-propagating states) and to probe efficiently the dynamics. These results provide a path towards the discrimination of the different transport pathways and to the characterization of environmental properties, enhancing our understanding of the role that coherent processes may play in biological complexes.

INTRODUCTION

Recent experimental work has provided evidence supporting the existence of long-lived electronic coherence during excitation energy transfer (EET) in photosynthetic complexes [1, 2]. Subsequent theoretical work has then highlighted the importance of an intricate interplay of noise and quantum coherence for the efficiency of excitation energy transfer (EET) in light harvesting complexes during photosynthesis and identified the crucial building blocks that underly this interplay [3–10]. While computer simulations and analytical work allow us to identify and verify the importance of these effects in theory, the experimental verification of their relevance in actual bio-molecular systems is still outstanding. One path forward towards this goal is the application of optimal control methods to the bio-molecular quantum dynamics in contact with environments with the aim of preparing specific initial states and control the subsequent dynamics. This would then allow for the generation of dynamical behaviour and hence signals that can lead to the biggest discrepancies between alternative theoretical hypotheses. Indeed, here we employ optimal control to develop different strategies that, when experimentally tested, will allow to enhance our comprehension of coherent processes in biological complexes.

Quantum coherent control drives a quantum system dynamics towards a specific goal by exploiting quantum coherence and interference effects [11]. Coherent control techniques have been proposed for photochemical and photobiological processes - see Refs. [12–17] for an overview on this topic. For instance, shaped light has been used to discriminate spectroscopically indistinguishable biochromophores through selective fluorescence depletion [18] and also to control energy flow in bacterial photosynthesis by increasing the amount of a triplet state signal in comparison to a singlet state signal in carotenoids [19]. The first evidence of control of exciton states in light-harvesting systems was presented experimentally in Ref. [20]. Moreover, to the best of our knowledge, the first attempt to use open-loop optimization to control the exciton dynamics of a light-harvesting system was theoretically provided in Ref. [21], however the control algorithm employed there imposed some limitations to their analysis: in particular their optimization was limited to state populations.

To overcome these limitations, we present and apply a recently introduced optimization algorithm (CRAB) [22]. In particular, we apply quantum (open loop) optimal quantum control theory to the dynamics of the electronic excitations in the Fenna-Matthews-Olson (FMO), a biological pigment-protein complex involved in the early steps of photosynthesis in green sulphur bacteria [1, 2, 23–25]. Specifically, by using the CRAB approach in the context of the FMO complex i) we achieve general state preparation: this will allow us to prepare specific initial states, especially fast and slow propagating states exhibiting constructive or destructive interference, ii) we explore experimental constraints and imperfections (adapted to the expected experimental setup [26]), iii) we optimize the difference in signals for different preparations to test theoretical hypotheses, and iv) we also discuss optimized probing of the system by optimal control of the readout pulses. Finally we provide an outlook discussing various possible extensions of our approach.

THE MODEL

In this section we present the basic ingredient of our theoretical model and fix the notation. The effective dynamics of the FMO complex can be modeled by a 7-qubit Hamiltonian describing the coherent exchange of excitations between chromophores or sites, i.e.

$$H_{fmo} = \sum_{j=1}^7 \hbar\omega_j \sigma_j^+ \sigma_j^- + \sum_{j \neq l} \hbar v_{j,l} (\sigma_j^- \sigma_l^+ + \sigma_j^+ \sigma_l^-)$$

where σ_j^+ (σ_j^-) are the raising (lowering) operators for site j , $\hbar\omega_j$ is the local site excitation energy, and $v_{j,l}$ denotes the hopping rate of an excitation between the sites j and l - see Ref. [5] for more details about this model. In the site basis, we follow [27] and employ the Hamiltonian matrix elements

$$H = \begin{pmatrix} 215 & -104.1 & 5.1 & -4.3 & 4.7 & -15.1 & -7.8 \\ -104.1 & 220.0 & 32.6 & 7.1 & 5.4 & 8.3 & 0.8 \\ 5.1 & 32.6 & 0.0 & -46.8 & 1.0 & -8.1 & 5.1 \\ -4.3 & 7.1 & -46.8 & 125.0 & -70.7 & -14.7 & -61.5 \\ 4.7 & 5.4 & 1.0 & -70.7 & 450.0 & 89.7 & -2.5 \\ -15.1 & 8.3 & -8.1 & -14.7 & 89.7 & 330.0 & 32.7 \\ -7.8 & 0.8 & 5.1 & -61.5 & -2.5 & 32.7 & 280.0 \end{pmatrix}$$

where the zero of energy has been shifted by 12230 cm^{-1} for all sites, corresponding to a wavelength of $\cong 800 \text{ nm}$ (all numbers are given in units of $\text{cm}^{-1} = 1.988865 \cdot 10^{-23} \text{ Nm} = 1.2414 \cdot 10^{-4} \text{ eV}$) – see Fig. 1. In a first approximation, and with the aim of identifying the main transport paths, the dissipation and dephasing caused by the surrounding environment are modeled by the following local Lindblad terms

$$\mathcal{L}_{diss}(\rho) = \sum_{j=1}^7 \Gamma_j [-\{\sigma_j^+ \sigma_j^-, \rho\} + 2\sigma_j^- \rho \sigma_j^+] \quad (1)$$

$$\mathcal{L}_{deph}(\rho) = \sum_{j=1}^7 \gamma_j [-\{\sigma_j^+ \sigma_j^-, \rho\} + 2\sigma_j^+ \sigma_j^- \rho \sigma_j^+ \sigma_j^-], \quad (2)$$

with Γ_j and γ_j being the dissipative and dephasing rates at the site j , respectively. In the following, we will consider the case in which the dephasing and dissipation rates are equal for all sites and labeled. As in Ref. [5], we denote the common rates as $\gamma = \gamma_j$ and $\Gamma = \Gamma_j = 5 \times 10^{-4} \text{ ps}^{-1}$ for site $j = 1, \dots, 7$. The latter corresponds to the measured lifetime of excitons which is of the order of 1 ns. Finally, the transfer efficiency into the reaction center is measured in terms of the population in the ‘sink’, numbered 8, which is populated by an irreversible decay process (with rate Γ_{sink}) from the site 3, as described by the Lindblad term

$$\mathcal{L}_{sink}(\rho) = \Gamma_{sink} [2\sigma_8^+ \sigma_3^- \rho \sigma_3^+ \sigma_8^- - \{\sigma_3^+ \sigma_8^- \sigma_8^+ \sigma_3^-, \rho\}] \quad (3)$$

where $\Gamma_{sink} \sim 6.3 \text{ ps}^{-1}$ (note that $\hbar \sim 5.3 \text{ cm}^{-1} \text{ ps}$). The transfer efficiency is given by $p_{sink}(t) = 2\Gamma_{sink} \int_0^t \rho_{33}(t') dt'$, with $\rho_{33}(t')$ being the population of site 3 at time t' . In the inset of Fig. 2, we show the behavior of p_{sink} as a function of the dephasing rate γ , at time $t \sim 10 \text{ ps}$, when one excitation is initially injected in site 1.

In order to describe the coupling between the FMO complex and a short laser pulse, typically used in the laboratory to irradiate it [1, 23, 24, 27], we add also a semiclassical time-dependent Hamiltonian term, $H_{FMO-laser}(t)$, which in rotating wave approximation takes the form

$$H_{las}(t) = - \sum_{i=1}^7 \vec{\mu}_i \cdot \vec{e} E(t) e^{-i\omega_l t} \sigma_i^+ + h.c. \quad (4)$$

where $\vec{\mu}_i$ is the molecular transition dipole moment of the individual site i [28], \vec{e} and ω_l are, respectively, the polarization and the frequency of the field, and $E(t)$ is the time-dependent electric field. In the following, we assume $E(t)$ having the form

$$E(t) = E_0 f(t),$$

with $E_0 = 15 \text{ D}^{-1} \text{ cm}^{-1} \sim 9 \cdot 10^7 \text{ V/m}$ (where in SI units the Debye is given by $D \sim 3.34 \cdot 10^{-30} \text{ C} \cdot \text{m}$), and a time-dependent modulation

$$f(t) = \frac{e^{-\frac{(t-t_0)^2}{2\sigma^2}}}{\lambda(t)} \frac{1 + \sum_{k=1}^m A_k \sin(\nu_k t) + B_k \cos(\nu_k t)}{1 + \sum_{k=1}^m |A_k| + |B_k|}, \quad (5)$$

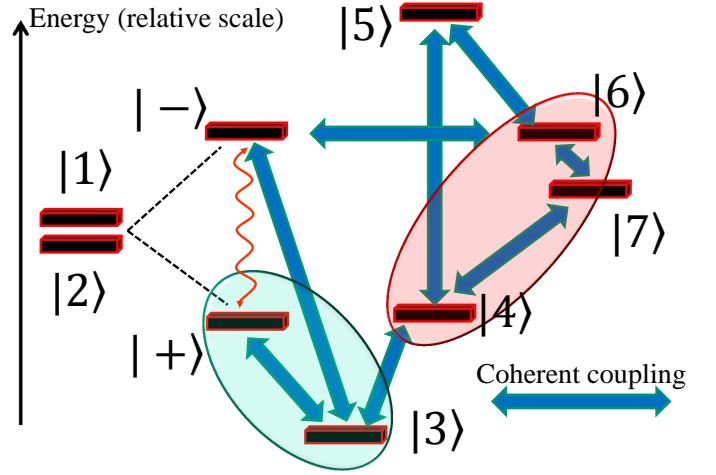


FIG. 1. FMO energy level structure where $|i\rangle$ denotes a single excitation in site i . The states $|\pm\rangle$ are the symmetric and anti-symmetric superpositions of the states $|1\rangle$ and $|2\rangle$. The green and red bubbles identify the fast and slow transport path, as detailed in Ref. [9] where the interplay between different transport pathways in FMO dynamics was discussed at length. The main effect of the inclusion of dephasing noise is the opening of an incoherent relaxation channel from level $|-\rangle$ to level $|+\rangle$ (red wiggled line) and therefore the effective suppression of the coherent oscillation between level $|-\rangle$ and sites 6-7-4 that dominates the coherent dynamics and is responsible of the very slow transport once the sink population has reached 50% (initial population held in site $|+\rangle$). The proposed quantum control strategies efficiently probe this dynamical model.

with a ramp factor $\lambda(t) = 1 + 5[e^{200(t-T)/T} + e^{-200t/T}]$ (such that $f(0) \sim f(T) \sim 0$), and A_k , B_k , and $\nu_k \equiv 2\pi kr/T$ being parameters to be optimized by using the method described below, where r is a random number, T is the time at which we want to prepare, for instance, some desired state. Moreover, we vary also the angles θ and ϕ of the polarization axis \vec{e} , with respect to the dipole moment of site 1, i.e. $\theta = \theta_1 + \Delta\theta$ and $\phi = \phi_1 + \Delta\phi$, with θ_1 and ϕ_1 describing the orientation of the site-1 dipole moment, and $\Delta\theta$ and $\Delta\phi$ being some free parameters. The dipole moments of the 7 FMO chromophores along the three reference axes are (in Debye D , where $1 D \sim 3.34 \cdot 10^{-30} \text{ C} \cdot \text{m}$):

BChl	X	Y	Z
1	-3.081	2.119	-1.669
2	-3.481	-2.083	-0.190
3	-0.819	-3.972	-0.331
4	-3.390	2.111	-1.080
5	-3.196	-2.361	0.7920
6	-0.621	3.636	1.882
7	-1.619	2.850	-2.584

In the following, we choose $m = 7$ and $T = 250 \text{ fs}$ and also chose the carrier frequency ω_l as an additional free parameter in the optimization. We have also worked with higher values of m , up to $m = 25$, which resulted in small fidelity enhancements (a few %) but resulted in longer optimization times.

As direct single site addressing is not possible in the FMO

complex due to the strongly overlapping lines we will apply quantum optimal control tools as described more carefully in the next section to shape the laser pulse, i.e. $E(t)$, and prepare the system in a desired physical state and control its transport dynamics. Let us point out already here, that the parametrization of the laser pulse has been chosen to include some additional constraints, related to typical constraints that can be expected in future experiment in this direction. In particular, we limit the laser power both due to experimental reasons and in order to avoid damage to the sample or cause strong saturation. We also impose a limit on the time resolution of the laser pulse, by means of a limit to the spectral width of the pulse, to ensure that it does not exceed 10 fs, since faster modulation of the laser is difficult to control experimentally.

OPTIMAL CONTROL: BACKGROUND AND METHOD

Coherent control of exciton states in light-harvesting systems was demonstrated experimentally in [20] and theoretically in [21]. In Ref. [20] feedback-optimized femtosecond pulses are applied to the LH2 antenna complex from *Rhodospseudomonas acidophila* and to a bioinspired artificial dyad molecule, in order to control the efficiency of the light-harvesting dynamics. Specifically, they optimize the branching ratio of energy transfer between intra- and intermolecular channels in the complex's donor-acceptor system and obtain an enhancement of about 30% in the LH2 system and about 10% in the artificial dyad molecule, by shaping the pulses employing feedback in an iterative learning loop scheme.

In all mentioned experimental demonstration of control of photochemical and photobiological processes [12–17, 20], closed-loop optimization by evolutionary algorithm was applied [29]. The procedure consists of three basic components: 1) a pulse shaper, generating the pulse shape to be tested, 2) the experiment, generating the feedback signal by pump-probe spectroscopy, 3) a computer, running the learning algorithm and driving the optimization. Hence, the closed-loop optimization proceeds along the following steps: i) a random guess of a set of pulses is shaped through the pulse shaper and then tested on the sample; ii) then the feedback signal is evaluated and used to start an evolutionary genetic algorithm (based on selection of 'parents', 'mutations', 'recombination', and 'generation' of new sets of pulse shapes); iii) a new set of pulses is obtained through the pulse shaper and applied to the sample. These steps will be repeated until the optimization has converged by following the so-called learning curve.

Despite the interesting applications of this technique, closed-loop optimization tends to be effective only for population control, while coherent control experiments cannot be performed because of the inherent shortcoming of transient absorption (TA) spectroscopy. One way to overcome this issue could be to use 2D electronic spectroscopy in order to get information about the phase, which is necessary as a feedback signal in coherent control experiments. Here, we solve this issue, using open-loop control approach: one first numeri-

cally optimizes laser pulses via numerical simulations and the applies them to the sample obtaining the desired result, for example, the experimental preparation of the sample in some desired state with very high fidelity.

The main advantages of the open-loop approach with respect to the closed-loop approach are two-folds. In the latter, the pulses are often very complex, highly structured, and very demanding to interpret: it is usually rather difficult to understand the real physical effect of such series of consecutive pulses on the system. This limits the understanding of the physical processes underlying a certain biological behaviour. Moreover, repeated closed-loop experiment rarely result in the same genetic algorithm-driven learning curve, increasing the difficulties of the analysis of the final optimal series and of the error estimation. On the other hand, in the open-loop scheme the optimally-shaped pulse is well determined and can be applied on the sample repeatedly to increase the signal to noise level and to compare the output feedback when changing the applied phase. It is then easier to find the explanation for the response of the system and the physical mechanism behind it. This problem becomes even simpler when the CRAB optimization is used as, as explained below, it results in optimal but very simple, robust and structured pulses. Let us stress however that the open loop technique can be applied directly only when the system parameters (e.g., Hamiltonian and environmental noise) are sufficiently well known and this, indeed, makes the closed-loop approach more feasible for several biological systems in which this information is not yet accessible. Here recently developed methods for quantum process tomography applied to multi-chromophoric systems, providing the decoherence of the system, the density matrix, as well as the Hamiltonian parameters [30] will be able to assist our open-loop approach. This is even more so as the robustness of the pulse shapes that we obtain from our open-loop technique allow us to use open loop scheme even if the system details are not well measured. Quite reasonably, the best scheme would be a combination of these two approaches. Indeed, one could use, for instance, closed-loop control as a means to obtain information about system parameters, e.g. if one optimizes the pulse in the experiment then one can chose this pulse and find out theoretically for which system parameters it reproduces the experimental data. Then, varying the target that is to be optimized, we obtain different pulses and can repeat this investigation; each time one obtains useful information about the system parameters. Working out such a programme might be useful as it might allow an alternative to tomography. Once we apply this procedure, by using the obtained information about the system, an open loop control can be then successfully applied.

The first work where open-loop optimal control in FMO complexes is reported in [21]. The authors investigate the control of exciton dynamics in FMO complex, by using polarized-shaped pulses optimized by means of a derivative functional equation for the target function. In particular, they use shaped pulses to optimize the excitation energy localization in a single chromophore of the FMO complex (site 7).

Here we extend and improve this result using the recently developed CRAB optimization technique (described below) targeting different initial states, to investigate different transport and decoherence processes in FMO. Moreover, we are able to consider faster processes that are more robust against decoherence as we optimize pulses of a few hundred femtosecond length. This allows us also to perform coherent control, i.e. preparation of a coherent superposition state, as well excitation energy localization. Concerning the case of single site preparation, it is not feasible to perform a clear comparison with the results of Ref. [21], since they studied the FMO antenna complex present in the *Chlorobium Tetidum* bacterium, while here we investigate the FMO complex found in a slightly different bacterium called *Prosthecochloris aestuarii*. However, from a general perspectives, it seems that our approach allows us to get much higher fidelity, and, more importantly, to use sensibly shorter laser pulse lengths (250 fs, while their optimal pulse are 600 fs long). These difference appear to be even more relevant and crucial when one wants to prepare a coherent state in presence of strong dephasing noise.

It should be noted that, since we are considering short pulse durations, neglecting the double-exciton states is a good approximation, also according to the theoretical results in Ref. [21]. Besides, the efficiency of the CRAB algorithm allow us to investigate more deeply the issue of random orientations of the FMOs in the sample by considering very large samples (10^4 FMOs), while in Ref. [21], due to computational limitations, only some preliminary results were reported. In fact, we will demonstrate that even a partial orientation of the samples by means of an external field combined with optimal pulses will improve experimental results significantly. Finally, we show also how to optimize the probe of the system to improve the experimental results even more.

To achieve all this here, we use the Chopped RANdom Basis (CRAB) optimization, introduced in Ref. [22], to optimize a specific figure of merit, e.g. population in some localized or delocalized state at some final time or the final fidelity with respect to a target state $\mathcal{F}(T)$, by varying the control field entering into the Hamiltonian term in Eq. (4). Introducing the control field parametrization given in Eq. (5) the functional becomes a multivariable cost-function $\mathcal{F}(\Delta\theta, \Delta\phi, \omega_l, t_0, \sigma, \{A_k\}, \{B_k\})$ on which any standard minimization method can be applied. We started with $\mathcal{O}(10^3)$ different initial random configurations and applied a direct search algorithm, which does not compute gradient nor Hessian, to find the function minimum [31]. To minimize an M -variable function, the Nelder-Mead algorithm starts defining a $M + 1$ dimensional polytope and then, in its simplest implementation, moves it replacing the worst point with a point reflected through the barycenter of the other M points, resulting in a (local) minimization of the function. We used the Subplex variant of the Nelder-Mead algorithm, which applies the same algorithm to different subspaces to improve the convergence [32]. The CRAB optimization strategy introduced above allows –as we shall show in the following– to find the

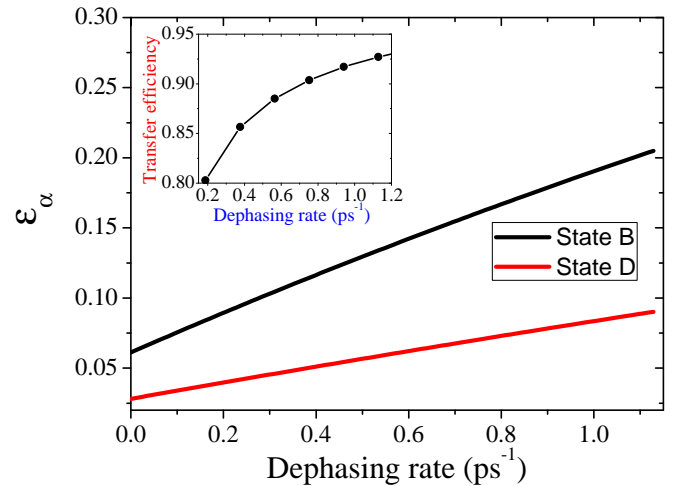


FIG. 2. ε_α versus dephasing rate γ (in units of ps^{-1}), for different prepared initial states. Specifically, our goal is to prepare the states B and D (i.e., $\alpha = B, D$). As described in the text, these quantities are given by $\varepsilon_B = 1 - \langle +|\rho|+ \rangle = 1 - \frac{\rho_{11} + \rho_{22}}{2} - \Re[\rho_{12}]$ and $\varepsilon_D = 1 - \rho_{5,5} - \rho_{6,6} - \rho_{7,7}$. Inset: Transfer efficiency vs. dephasing rate γ (uniform for all the sites) at $t = 10$ ps, when one excitation is initially in site 1.

optimal pulses to extremize the desired figure of merit: it is efficient and versatile as it does not need any analytical solutions of the system dynamics, it does not compute gradients and can be easily adapted to different figure of merits. More importantly, it includes already many experimental constraints such as the finite band-width and power of the control pulses. Finally, we mention that optimal control pulses are quite robust with respect to system parameters perturbation and noise up to a few percent, as shown in the literature in different scenarios (see e.g. [33, 34]). This robustness arise from the fact that the optimal dynamics lies in a minima of the functional to be extremized, thus first order perturbations vanish.

INITIAL STATE PREPARATION

In Ref. [9], it has been found that the coherent transfer of the electronic excitation energy in the FMO complex takes place essentially through two different pathways: one mediated by the state $|+\rangle$, which is shifted towards site 3 and leads to very fast transfer to the reaction center, and a second one, involving the sites 5, 6 and 7, which is comparatively slow because of the energy gap with the site 3 and because the excitation suffers many coherent oscillations between those sites before reaching site 3. Indeed, the presence of dephasing noise assists the transport because, on the one hand, it opens up a new additional pathway, i.e. incoherent tunneling between the state $|-\rangle$ and $|+\rangle$, and, on the other hand, it partially suppresses the transition from $|-\rangle$ to sites 5, 6, 7, and also leads to fast incoherent oscillations between those three sites before reaching the sink. Motivated by these results, we apply the CRAB optimization to find the optimal pulses to

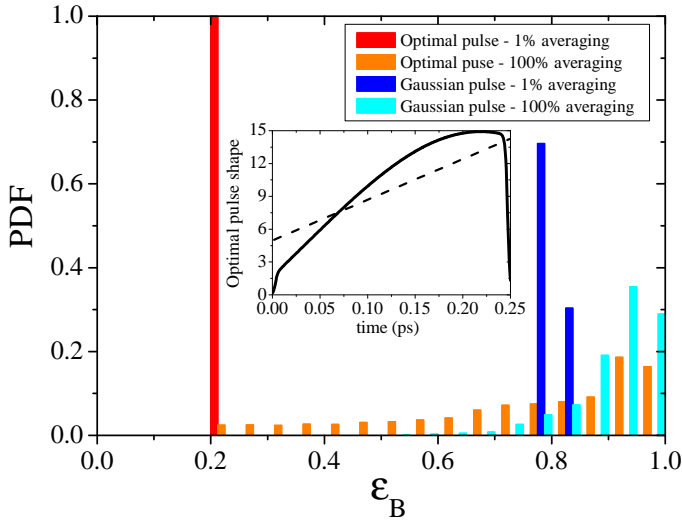


FIG. 3. Probability distribution of the quantity ε_B for the preparation of the state B , in the presence of dephasing with rate $\gamma \sim 1 \text{ ps}^{-1}$, by using the optimal and a standard Gaussian laser pulse. We considered a sample of 10^4 FMO complexes to get enough statistics. Inset: shape of the optimal pulse, optimized to prepare the state B in 250 fs. Notice that the laser pulse amplitude is always shown in units of $D^{-1} \text{ cm}^{-1} \sim 6 \cdot 10^6 \text{ V/m}$. Finally, the optimal values of the other free parameters are $\Delta\theta = 2.5$, $\Delta\phi = 7.6$, and $\omega_l = 121.76 \text{ cm}^{-1}$, and we find $\varepsilon_B = 0.20$, without averaging. Interestingly enough, by considering a simpler linear shape (dashed line), we find a quite similar error, i.e. $\varepsilon_B = 0.24$, by showing the ‘robustness’ of the pulse shape to prepare the state B .

selectively prepare a state $|D\rangle$ with maximum probability of finding the electronic excitation in the sites $|5\rangle, |6\rangle, |7\rangle$ (dark or non-propagating state) and $|B\rangle \equiv |+\rangle = (|1\rangle + |2\rangle)/\sqrt{2}$ (bright or propagating state). We consider the full model for the FMO complex (described before), but in absence of reaction center, since it is usually the case in the current experiments on this light-harvesting system. However, the presence of the sink would not affect the state preparation process since the laser pulse is applied for a very short laser pulse. This is also confirmed by the analysis on the transport pathways discussed below. In particular, we apply the CRAB strategy to prepare the FMO complex (initially in the ground state) in the desired state after $t = 250 \text{ fs}$ during which we excite the system with a laser pulse. We maximize the probability of finding the excitation in the desired state (B or D), that is our figure of merit, by minimizing the following quantities

$$\varepsilon_B = 1 - \langle +|\rho|+ \rangle = 1 - \frac{\rho_{11} + \rho_{22}}{2} - \Re[\rho_{12}], \quad (6)$$

$$\varepsilon_D = 1 - \rho_{5,5} - \rho_{6,6} - \rho_{7,7}. \quad (7)$$

In Fig. 2 results of the optimization are shown as a function of the dephasing rate present in the system. As it can be seen, increasing the amount of dephasing in the dynamics, the error ε_α increases in both cases.

As remarked earlier, the so achieved pulses are quite robust against changes in system parameters such as the environmental noise level. To demonstrate this we apply the following

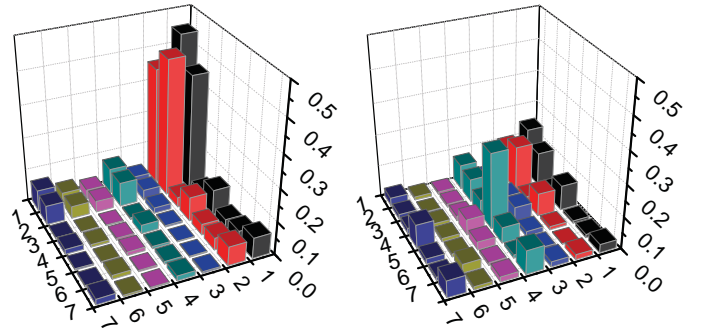


FIG. 4. Modulus of the ensemble average of the elements of the FMO density matrix in the site basis (over 10^4 samples), after applying the optimal laser pulse to prepare the system in the state B . We introduce also static disorder, set to 1% (left) and 100% (right), and we get a fidelity for the desired state equal to 89% and 49.8%, respectively.

procedure. We find the optimal laser pulse in the presence of dephasing with rate $\gamma \sim 1 \text{ ps}^{-1}$. Then, we repeat the optimization with different values of dephasing and find, in general, only slightly different pulse shapes that result in values of error ε_α , which differ only slightly, less than 10^{-2} , from those obtained for the optimal shapes we found for dephasing $\gamma \sim 1 \text{ ps}^{-1}$. In other words, the same optimal pulse can be used to prepare some desired state irrespective of the strength of the dephasing noise in the dynamics is. These pulses are shown in the insets of Figs. 3 and 5. Let us also point out that, by considering a simpler linear pulse shape (interpolating the optimal pulse, see dashed line in the inset of Fig. 3), one obtains a very similar error, whose difference is less than 0.05 in both cases (D and S states). As the optimal pulse shapes depend only marginally on the noise level, the results in Fig. 2 can become a tool to obtain information about the noise strength in the FMO dynamics by measuring the quantity ε_α . Notice also that, removing the experimental constraints on the pulse shape – namely the limit on the maximal pulse intensity and the time resolution – it is possible to find near-unit fidelity for any state and any value of the dephasing rate. For instance, if one allows twice as high field strength, an improvement of even several % for the fidelity can be obtained.

In realistic samples, the orientation of the FMO complexes does exhibit significant disorder. Hence it is crucial to consider the effect of the effect of random orientation of the FMO complexes which leads to an ensemble average over the random distributions. In particular, we consider two extreme cases in which we add 1% and 100% of random disorder, i.e. $\theta = \theta_{opt} + \eta s_1$ and $\phi = \phi_{opt} + \eta s_2$, where θ_{opt} and ϕ_{opt} are the optimal values, $s_{1,2}$ are random numbers in the range $[0, 2\pi]$ and $\eta = 0.01, 1$ respectively. As illustrated by the results in Figs. 3 and 5, the corresponding distributions are fairly distinguishable. Indeed, for the state B analyzed in Fig. 3, the ensemble averages of ε_B are 0.207 and 0.751, respectively for 1% and 100% of orientation disorder, in the case of the optimal pulse, while they are 0.793 and 0.904 in the Gaussian one, respectively. On the other hand, for the state

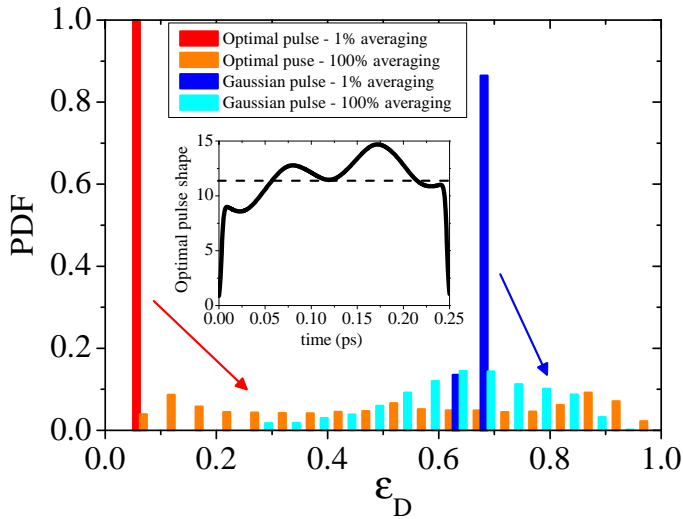


FIG. 5. Probability distribution of the quantity ε_D for the preparation of the state D , in the presence of dephasing with rate $\gamma \sim 1 \text{ ps}^{-1}$, by using the optimal and a standard Gaussian laser pulse. As before, since in the lab one has a sample of FMO complexes in random orientations, we plot these pdfs for two extreme cases in which we add 1% and 100% of random disorder to the two angles defining the orientation of the FMO complex. Inset: shape of the corresponding optimal pulse. The optimal values of the other free parameters are $\Delta\theta = 3.09$, $\Delta\phi = 3.76$, and $\omega_l = 504.46 \text{ cm}^{-1}$, and we find $\varepsilon_D = 0.09$, without averaging. By considering a much simpler constant laser field (dashed line), one still gets a very good preparation of the state D , i.e. $\varepsilon_D = 0.10$.

D analyzed in Fig. 5, the distribution averages are, respectively, 0.091 and 0.531 in the case of the optimal pulse, and 0.663 and 0.634 in the Gaussian one. Moreover, the modulus of the ensemble average of the elements of FMO density matrix in the site basis, after the state preparation by means of the optimal pulse and the Gaussian one, are shown in all the analyzed cases (in presence of static disorder) in Figs. 4, 6, 7. Furthermore, we measure the fidelity $F(\rho, \sigma)$ between the desired state σ and the one ρ achieved by optimal control as $F(\rho, \sigma) = \text{Tr}[\sqrt{\sqrt{\sigma}\rho\sqrt{\sigma}}]$. Notice that, in the case of state

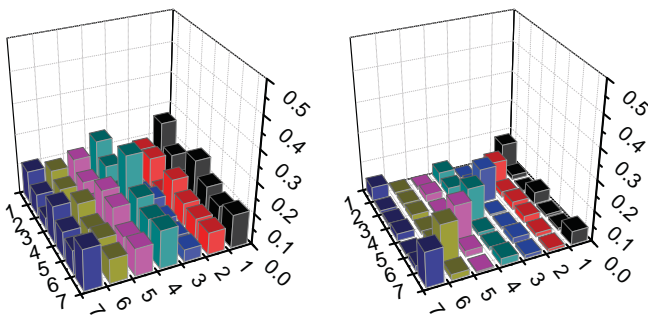


FIG. 6. Modulus of the ensemble average of the elements of the FMO density matrix in the site basis (over 10^4 samples), after applying a standard Gaussian pulse. We consider also the presence of static disorder, which is set to 1% (left) and 100% (right), respectively.

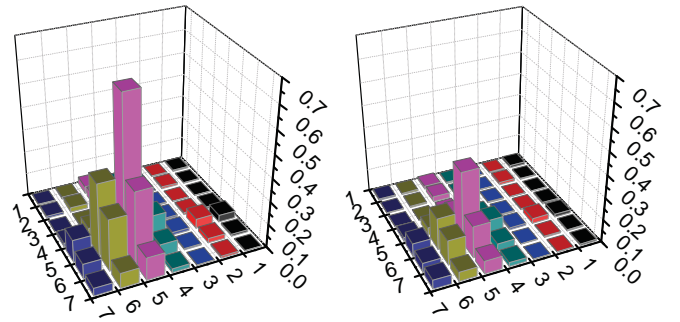


FIG. 7. Modulus of the ensemble average of the elements of the FMO density matrix in the site basis (over 10^4 samples), after applying the optimal laser pulse to prepare the system in the state D . Again, the static disorder is set to 1% (left) and 100% (right) and we get a fidelity for the desired state equal to 86% and 63.1%, respectively.

D , since the quantity ε_D is defined only in terms of the total population in site 5, 6 and 7, in order to calculate the fidelity, we need to specify a particular goal state σ . For simplicity, we choose a target state with 70% population in site 5, 25% in site 6, 5% in site 7, and vanishing coherences. This distribution of populations is similar to the one obtained when minimizing the quantity ε_D . In Fig. 4, we notice that, if one will be able, in the lab, to orientate very well the FMO complexes in the sample, the state B is prepared with very high fidelity. Additionally, when the FMO complexes are completely randomly oriented in the sample, the fidelity is much lower. Indeed, one observes a large amount of population in site 4 which is almost in resonance with the site 1 and 2. However, this does not affect the transport pathway discrimination (as shown below), because the population in site 4 goes quickly to the site 3 as well as the state B . A similar behaviour is observed for the preparation of the state D . Nevertheless, in this case the high values of the fidelity are more robust to the introduction of orientation disorder, since one wants only to populate the high-energy sites 5, 6 and 7 neglecting any control of the phase terms. Instead, in Fig. 6, one clearly observes that a gaussian laser pulse is not able to selectively prepare specific states. Furthermore, when 100% of orientation disorder is considered, the gaussian pulse does almost equally populate all the sites with vanishing cross-term correlations (completely mixed state). Finally, it is worth pointing out that an experimental partial orientation of the sample will be able to sensibly enhance these fidelities, as shown below in the section about the orientation. In the following, we will use these optimal laser pulses, found to prepare those selected states, in order to investigate the different transport pathways in the FMO complex dynamics.

STATE PREPARATION DEPENDENT TRANSPORT

We now compare the transfer efficiency into the reaction center corresponding to the two different initial states that we have introduced before, including the Lindbladian term in Eq.

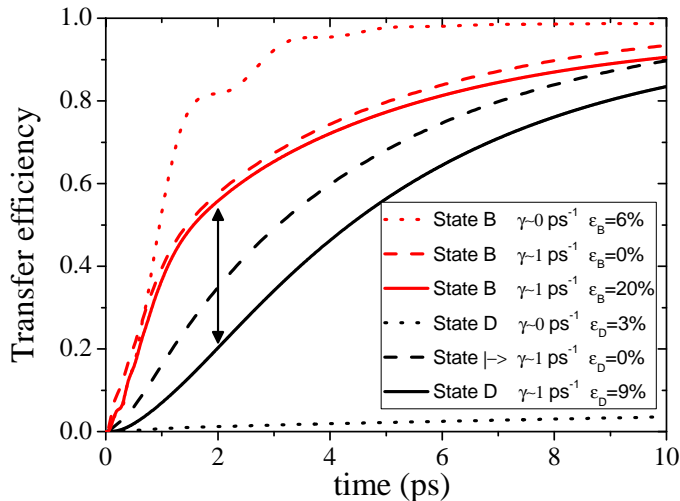


FIG. 8. Transfer efficiency as a function of time (ps) for different initial states, i.e. $|D\rangle$, $|-\rangle$ and $|B\rangle$, for two different values of dephasing rate $\gamma = 0$ and $\gamma \sim 1 \text{ ps}^{-1}$. Moreover, in one case, we consider also an idealized preparation of the state, i.e. $\varepsilon_\alpha = 0$. In the other cases, we consider the more realistic scenario when in the lab one prepares similar states applying the optimal laser pulses, in absence and presence of dephasing noise.

(3) – see Fig. 8. Notice that now the sink is included in the dynamics from the beginning, even if the optimal pulses were obtained without sink. Indeed, as discussed also above, it does not sensibly affect the state preparation since the pulse is applied for a very short time scale compared to the transfer rate from the site 3 to the reaction center.

In the absence of dephasing noise, as expected from the results in Ref. [9], the population initially prepared in sites 5, 6 and 7 is basically trapped and only very slowly gets into the reaction center, while the state $|+\rangle$ is almost in resonance with the site 3 and the transfer rate to the sink is much faster. However, increasing the amount of dephasing, these destructive interference effects are reduced, destroying the so-called invariant subspaces or dark states (see Ref. [5] for more details), and the efficiency discrepancy between the fast and the slow pathways decreases, as shown in Fig. 8. Particularly, the ratio fast/slow pathway transfer efficiency is about 2.5 for $\gamma \sim 1 \text{ ps}^{-1}$ and about 80 for $\gamma = 0$, at time $t = 2 \text{ ps}$. These results are particularly robust against various possible experimental inaccuracies: In Fig. 8 we show that, although the state preparation by the optimal laser pulse is not perfect, the corresponding behaviour is still good enough to distinguish the slow and fast transport pathways, compared to the case in which the specific states are exactly set in the numerical simulation. In other words, it turns out that, even if the state preparation is not perfect, one finds a very similar behavior for the transfer efficiency. This fact is fundamental to reproduce these results in the laboratory since the experimental fidelities will be smaller than the theoretical ones. Finally, we also consider the realistic experimental scenario in which a very large ensemble of FMO molecules is studied simultaneously in the

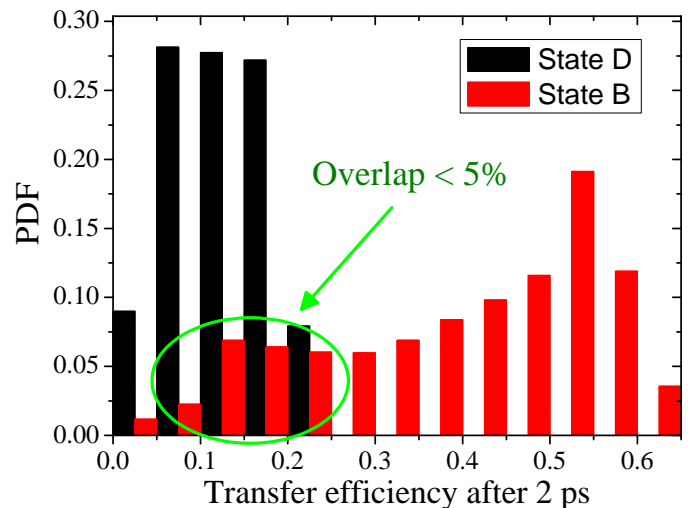


FIG. 9. Probability distribution of the transfer efficiency into the sink after 2 ps, in the presence of local dephasing with rate $\gamma \sim 1 \text{ ps}^{-1}$, for the optimal preparations of the state D and the state B , with 100% of random disorder in the orientation of 10^4 FMO complexes. The two distributions are distinguishable with less than 5% of error.

lab with different random orientations. It turns out that, even with 100% of random disorder in the orientations of the FMO molecules, the difference between the transfer efficiency after 2ps of the ‘dark’ and ‘bright’ states is still measurable. Indeed, as shown in Fig. 9, the two distributions of transfer efficiency are distinguishable with less than 5% of error. The ensemble averages are around 0.12 in the case of the state D , and 0.39 for the state B . In conclusion, the proposed analysis appears to be observable in a real experiment.

OPTIMAL CONTROL PULSE FOR EXPERIMENTS ON DIFFERENTLY ORIENTED SYSTEMS

In the lab one generally has a sample of many FMO complexes with random orientations and, hence, the laser pulse could be optimized also taking it into account.

In order to cover almost isotropically all the different orientations of the photosynthetic system in the sample, we consider the 20 directions pointing to the 20 vertices of a dodecahedron, and we optimize the pulse in order to minimize the quantity ε_α averaged over a sample of 20 differently oriented FMO complexes. Notice that the computational efficiency of the CRAB algorithm allows us to consider a much higher number of directions and we consider here only 20 just for simplicity and for illustration purposes. Indeed, the time complexity of such algorithms scales linearly with the number of orientations to average over and the optimization in the case of 20 directions takes only a time of the order of hours on a single standard CPU.

In Fig. 10, we show the probability distribution for ε_D when this new optimal pulse is applied to a sample of 10^4 FMOs in random orientations. As comparison, we plot also

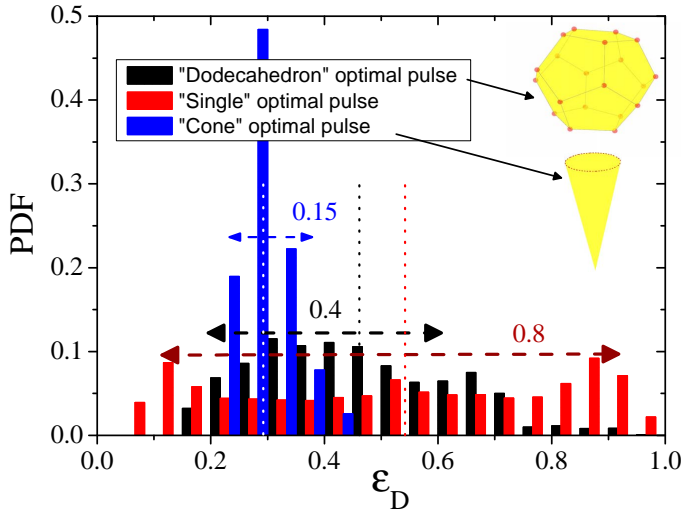


FIG. 10. Probability distribution of the quantity ε_D for the preparation of the state D , in the presence of dephasing with rate $\gamma \sim 1 \text{ ps}^{-1}$, by using the optimal pulses obtained by averaging on a single FMO complex with a specific orientation (as in Fig. 5), by averaging on a small sample of 20 (almost isotropic) FMO orientations pointing the 20 vertices of a dodecahedron, and on a sample of 21 orientations inside a cone with an opening angle of 0.1π . Hence, one considers the probability distribution of ε_D when these optimal pulses are applied to a sample of 10^4 FMO complexes in completely random orientations in the first two cases and, for the last case, randomly oriented inside that cone. The shape of the corresponding optimal pulses are similar to the one in the inset of Fig. 3. Moreover, we find, for the dodecahedron case, $\Delta\theta = 2.66$, $\Delta\phi = 2.61$, $\omega_l = 277.10 \text{ cm}^{-1}$, while, for the cone case, $\Delta\theta = -2.21$, $\Delta\phi = 1.86$, $\omega_l = 274.87 \text{ cm}^{-1}$. The dashed lines represent the corresponding averaged values, i.e. 0.53 (single orientation), 0.46 (dodecahedron), 0.29 (cone). The corresponding distribution widths are also plotted.

the corresponding probability distribution when we instead apply the optimal pulse used in Fig. 5. It turns out that this new pulse is somehow more robust and provides an error distribution whose width is about one half of the one obtained with the pulse optimized with a single FMO system. This could suggest a way to improve the state preparation of the FMO complex in the real experiment where one has a sample containing many FMO molecules in a solution. However, concerning the preparation of the more delicate state B this technique does not provide any noticeable improvement. Moreover, regarding the transport properties, the results are similar to those presented in Fig. 9 and the overlap of those two distributions is still less than 5% but does not decrease further. Notice that this overlap is already rather small to be able to be experimentally observed. Finally, we consider an intermediate case in which the FMO complexes can be partially oriented along a cone-shaped orientations. In particular, we repeat the analysis above but for 21 directions inside a cone with a 10% opening angle, i.e. 0.1π , and we optimize the pulse in order to minimize the quantity ε_α averaged over 21 FMO complex evolutions. Then, we apply this optimal pulse to a sample of 10^4 FMOs in random orientations inside this cone and we cal-

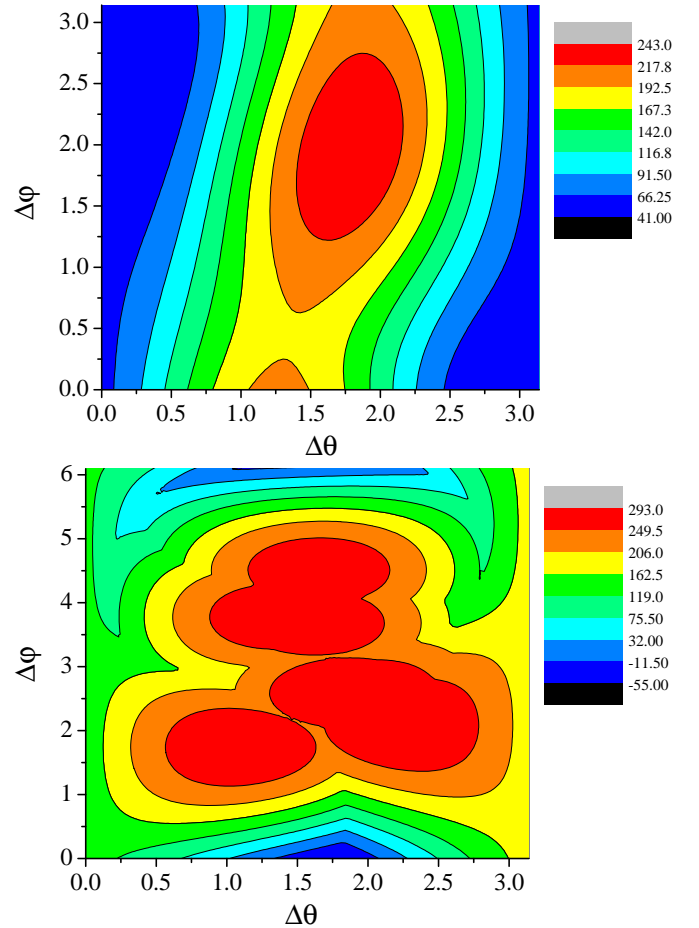


FIG. 11. Top: Behaviour of the quantity Δ (defined in the text), in units of cm^{-1} ($\sim 0.1 \text{ meV}$) as a function of the angles $\Delta\theta$ and $\Delta\phi$ defining the orientation of the FMO complex, in the case of $\omega_l = -1000 \text{ cm}^{-1}$ and $E_0 = 70 \text{ D}^{-1} \text{ cm}^{-1} \sim 42 \cdot 10^7 \text{ V/m}$. The difference between the maximum and the minimum value is comparable to the thermal energy and the maximum is obtained for $\Delta\theta \sim 1.75$ and $\Delta\phi \sim 2$, which seems to be the preferred orientation when the sample is subjected to this constant laser field. Bottom: maximum value of the Rabi frequencies $\vec{\mu}_i \cdot \vec{e}E_0$ versus $\Delta\theta$ and $\Delta\phi$. Notice that the values of the detunings are much larger than the Rabi frequencies.

culate the probability distribution for ε_D - see Fig. 10. We find that the width of the error distribution is further squeezed and shifted to smaller errors, i.e. higher fidelities.

TOWARDS THE ORIENTATION OF THE FMO SAMPLE

Here, we show how one could try to orientate the FMO systems in the experimentally available sample, by using some simple classical mechanics arguments. Following Ref. [35], we model each monomer of the FMO complex as a disk, whose mass and radius can be reasonably estimated to be equal to $M \sim 80 \text{ kDa} \sim 15 \cdot 10^{-23} \text{ Kg}$ and $R = 2 \text{ nm}$ (including the protein scaffolding). The corresponding moment

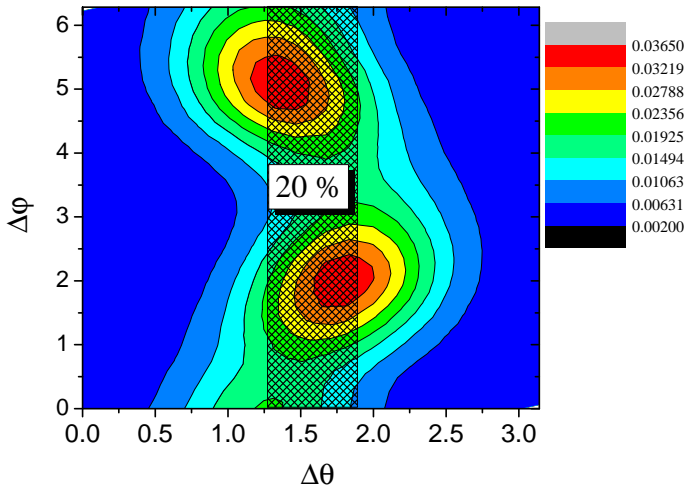


FIG. 12. Boltzmann-Gibbs probability distribution in orienting the FMOs in the sample, as a function of the angles $\Delta\theta$ and $\Delta\phi$, in the case of $\omega_l = -1000 \text{ cm}^{-1}$ and $E_0 = 70 \text{ D}^{-1} \text{ cm}^{-1}$. The dashed area represents the region in which we will sum up all the probabilities in the case, for instance, of a 20% cone opening angle, as shown in Fig. 13. Notice, however, that a slightly tilted strip would get higher probability for the same width and so further improves our results. The Gaussian pulse shape, used as comparison in the population behavior, is also shown (dashed line).

of inertia (with respect to one of its diameters as rotational axis) is hence $I = \frac{1}{4}MR^2 \sim 1.125 \cdot 10^{-31} \text{ Kg m}^2$. The rotational energy is $E = \frac{1}{2}I\omega^2$, with ω being the angular velocity in radians per second, i.e. the derivative of the angle rotated with respect to time $\omega = \frac{d\theta}{dt}$. At room temperature, by neglecting the friction due to the presence of a solution and, possibly, other more sophisticated effects, just to get an initial rough estimation, the time t_{rot} it takes for the system to rotate by an angle $\pi/2$ (which is roughly the average angle by which a complex has to be rotated) is trivially given by $t_{rot} = \frac{\pi}{2} \sqrt{\frac{I}{2E_{th}}} \sim 6 \mu\text{s}$, with $E_{th} \sim 25 \text{ meV}$ being the thermal energy. Actually, given that the disk will carry out a sort of random walk, the rotation time could be much longer than what is estimated here by means of this simple analysis.

Moreover, we investigate the energy landscape as a function of the orientation of the FMO complex, when is subjected to a constant electric field E_0 polarized along the axis \vec{e} with carrier frequency ω_l , i.e. the following quantity

$$\Delta = \sum_{i=1}^7 \frac{|\vec{\mu}_i \cdot \vec{e} E_0|^2}{\omega_i - \omega_l}. \quad (8)$$

By varying the orientation of the FMO complex in terms of the two angles θ and ϕ , the energy difference between the maximum and the minimum value is comparable to the thermal energy and one gets the maximum for $\Delta\theta \sim 1.75$ and $\Delta\phi \sim 2$ – see Fig. 11. The other parameters are chosen as $\omega_l = -1000 \text{ cm}^{-1}$ and $E_0 = 40 \text{ D}^{-1} \text{ cm}^{-1}$. Finally, following the simple reasoning above, we explicitly calculate how many FMO systems can be oriented around some direction at

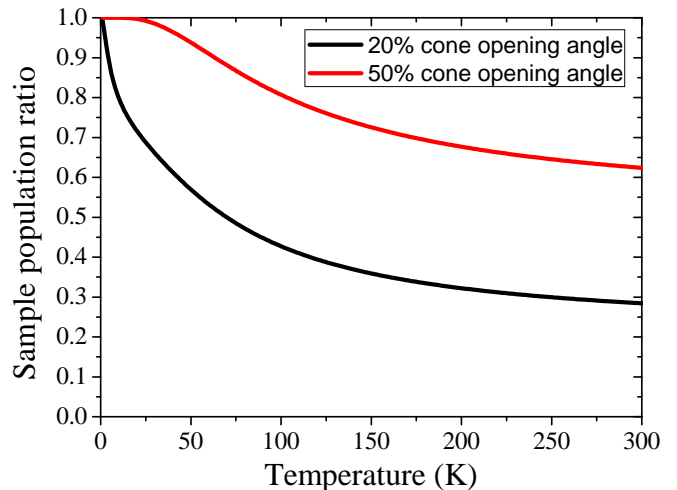


FIG. 13. Sample population ratio of FMOs oriented within a cone with some opening angle (20%, i.e. 0.2π , and 50%, i.e. 0.5π), as a function of temperature (K), with $\omega_l = -1000 \text{ cm}^{-1}$, and $E_0 = 70 \text{ D}^{-1} \text{ cm}^{-1}$, according to the Boltzmann-Gibbs distribution.

a certain external temperature, since the thermal fluctuations will unavoidably try to disorientate the sample. To do this, we calculate the probability for the FMO to be oriented at a certain angle by assuming that they follow a Boltzmann-Gibbs distribution, in the presence of a constant electric field – see Fig. 12. Then, by using the obtained probability distribution, we also evaluate how many FMO systems are oriented within a cone with a certain opening angle as a function of the temperature and for different values of opening angle. The corresponding results are shown in Fig. 13. By decreasing the temperature, the amount of oriented FMO systems in the sample increases and this would give us higher fidelities in the state preparation analysis and for the other related results above. Therefore, it seems feasible to orientate the FMO complexes in the sample to some extent using far detuned laser light. The

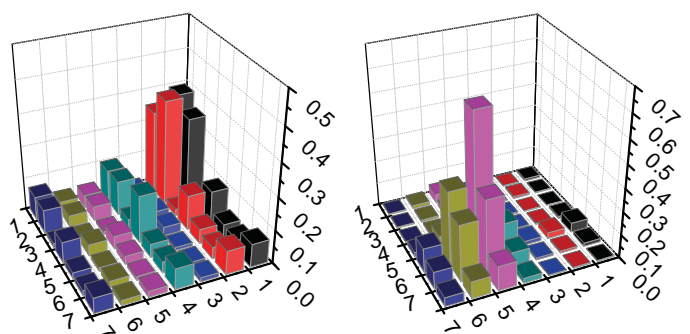


FIG. 14. Modulus of the ensemble average of the elements of the FMO density matrix in the site basis (over 10^4 samples), after applying the optimal laser pulse to prepare the system in the state B (left) and D (right), respectively. We introduce a static disorder, set to 10% in both cases, considering that some orientation will be obtained in the experiment. The fidelity for the preparation of state B and D are 74.4% and 85.1%, respectively.

typical individual optimal control experiments take of the order of \sim ps which, importantly, are several orders of magnitude shorter than the time for the FMO complexes to loose orientation after the detuned laser beam has been switched off. Hence, we can avoid interference between the orientation laser and the actual optimal control experiment. Finally, let us point out that a partial orientation of the sample will allow one to sensibly improve the state preparation results shown above - see Fig. 14. Indeed, a net improvement is observed, when compared to the 100% disorder case shown in Figs. 4 and 7.

OPTIMAL PROBE

In the context of controlling a molecular systems by optimal femtosecond laser pulses, a similar approach can be reasonably used to optimize the probe pulse absorption in a pump-probe scheme. A successful demonstration of the optimization of the absorbance of the probe pulse by optimal control techniques, but based on a derivative functional equation, was shown for a prototypical molecular three level system in Ref. [36]. Here, we repeat the analysis above for a probe laser pulse applied to the FMO complex by using the CRAB algorithm. In order to compare our theoretical predictions, e.g. in Fig. 9, with the experimental data, since there is no reaction center in the FMO complex sample used in the lab, one has to measure the population in site 3 as a function of time and then calculate the corresponding transfer efficiency, as defined in the model in Eq. (3). To do that, a probe laser pulse is applied to the sample and the corresponding absorption intensity is detected. Usually, the probe pulse is a Gaussian laser pulse on resonance with the site whose population one wants to measure, e.g. site 3. Here, we apply the optimal control tools to analyze whether a shaped pulse can detect the site population, particularly in site 3, with an higher ‘resolution’, as compared to a simpler Gaussian pulse. Actually, it will turn out that, when one considers only a single FMO complex, very high fidelity (99%) are already obtained by a gaussian pulse oriented along some optimal polarization axis and the pulse shaping will not give significant improvements. On the other side, if one has a sample of fully randomly oriented systems, both gaussian and an optimally shaped pulse bring to very low fidelities since the orientation disorder is too strong. However, if a partial orientation will be feasible from the experimental point of view, the control on the pulse shape sensibly increase the probability of successfully probing site 3. Specifically, we use the model above for a single FMO complex and we consider the case where initially all the population is in site 3 and we want to find the pulse which is able to detect this population by absorption, i.e. by removing population from the site 3. To apply the optimal control approach as defined above, we use the following error function

$$\varepsilon_P = \rho_{33}, \quad (9)$$

with ρ_{33} being the site-3 population.

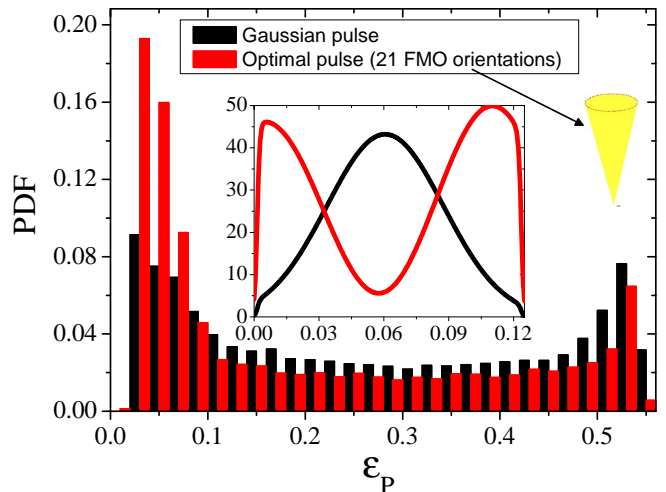


FIG. 15. Probability distribution of the quantity ε_P , when the FMO is initially prepared with all the population in site 3 and then subjected a laser probe pulse for a time interval of 125 fs to detect the site-3 population, in the presence of dephasing with rate $\gamma \sim 1 \text{ ps}^{-1}$. In particular, we consider the case of a Gaussian pulse on resonance with the site 3, i.e. $\omega_l = 0 \text{ cm}^{-1}$, and polarized along the optimal (wrt a single FMO) orientation, i.e. $\Delta\theta = 2.92$, $\Delta\phi = 1.85$, and the case of an optimal pulse obtained by averaging the error function ε_P over 21 directions inside a cone with an opening angle of 0.1π , whose optimal parameters are $\Delta\theta = 5.61$, $\Delta\phi = 1.39$, $\omega_l = 12.63 \text{ cm}^{-1}$. To get the probability distribution, we apply both pulses to a sample of 10^4 samples randomly oriented inside that cone. Inset: shape of both (Gaussian and optimal) probe pulses.

Moreover, the pulse is applied for a time interval of $t = 125$ fs. We find that, if there is just one FMO complex in the sample, the optimization will simply orientate the probe pulse polarization axis along some optimal direction (related to the site 3 dipole moment). Apart from the polarization control, the further optimization of the pulse shape does not bring further significant gains. Hence a Gaussian pulse will reliably detect the site-3 population (absorption efficiency, i.e. $1 - \varepsilon_P$, of 99%). However, if one applied this Gaussian pulse polarized along this optimized direction to a sample of randomly oriented FMOs, the absorption efficiency shows an almost flat probability distribution in the range $[0.45, 0.99]$, which is actually a bit higher for smaller efficiencies, i.e. the method does not provide us with a more efficient absorption signal (compared to the traditional way), and has associated an error of about 50%. If we apply the optimal control algorithm to find the best probe, averaged over 20 isotropic orientations according to the dodecahedron above, this does not improve sensibly the results either (data not shown). Finally, we consider the case in which the sample is partially oriented, particularly within a cone of 0.1π opening angle, and we optimize the pulse along 21 orientations inside this cone, as done above for the pump. Hence, we apply this optimally shaped pulse to a sample of 10^4 FMOs randomly oriented inside this cone and we compare the absorption efficiency to the case of a Gaussian pulse, polarized along the optimal orientation obtained for a

single FMO. We find that the optimally-shaped pulse gives a probability of high absorption efficiency (small ε_P), which is more than twice larger than the one with a Gaussian pulse - see Fig. 15. Therefore, in presence of structural disorder but achieving a partial orientation of the FMOs in the sample, both polarization and shape optimizations may enhance the probe pulse absorption in a pump-probe scheme, which is crucial for an efficient discrimination of dynamical properties, like the identification of transport paths discussed here.

SUMMARY AND PROSPECTS

In summary, the experimental verification in bio-molecular systems of fundamental building blocks of quantum dynamics in presence of environment [3–10] requires the development of novel experimental tools and theoretical methodology. In this work we have contributed to this effort with the demonstration that novel methods from the theory of optimal control can be combined with ultra-fast laser pulses to provide enhanced diagnostic tools suggesting promising new routes for experiment. In particular we have introduced and applied the CRAB technique for optimal quantum control that was originally developed in quantum information science [22] and used it to determine, for realistic experimental parameters [26], pulse shapes that allow for the preparation of arbitrary coherent superpositions with high fidelity. We are also able to reduce the impact of the random orientation of FMO complexes in typical samples and we are able to optimize the read-out of the system to maximize state sensitivity. Finally, we indicated that, in a future experiment applying this approach, a comparison of our theoretical calculations with experimental data, would allow us to extract information about the largely unknown details of the system-environment interaction, thus complementing recently proposed methods based on tomography [30]. These methods may support the experimental confirmation that recent models concerning the interplay of transport processes and environmental noise [3–10] grasp the main features of the system dynamics.

In future work, based on the techniques presented here, we are planning to consider more general non-Markovian models [37–40], other bio-molecular complexes and we will explore the importance of multiple excitations in the system. We will also explore the use of CRAB as a tool for closed-loop control in this context. These tools will then be applied to provide optimized experimental set-ups that explore questions concerning the relevance of quantum coherence and decoherence in the dynamics of bio-molecular systems. This includes the quantitative probing of the functional relevance of quantum coherence and entanglement, the exploration of which would shed further light on the question whether entanglement is a necessary ingredient for excitation energy transport.

We acknowledge discussions with Jon Marangos concerning experimental parameters. This work was supported by

the EU Integrating projects Q-ESSENCE and AQUITE, the EU STREP project CORNER, SFB/TRR21, and the Alexander von Humboldt Foundation. F.C. was supported also by a Marie-Curie Intra-European Fellowship within the 7th European Community Framework Programme. We acknowledge the bwGRiD for computational resources.

-
- [1] G.S. Engel, T.R. Calhoun, E.L. Read, T.-K. Ahn, T. Mančal, Y.-C. Cheng, R.E. Blankenship, G.R. Fleming, *Nature* **446**, 782 (2007).
 - [2] G. Panitchayangkoon, D. Hayes, K.A. Fransted, J.R. Caram, E. Harel, J.Z. Wen, R.E. Blankenship, G.S. Engel, *Proc. Nat. Acad. Sci.* **107**, 12766 (2010).
 - [3] M. Mohseni, P. Rebentrost, S. Lloyd, and A. Aspuru-Guzik, *J. Chem. Phys.* **129**, 174106 (2008).
 - [4] M.B. Plenio and S.F. Huelga, *New J. Phys.* **10**, 113019 (2008).
 - [5] F. Caruso, A.W. Chin, A. Datta, S.F. Huelga, and M.B. Plenio, *J. Chem. Phys.* **131**, 105106 (2009).
 - [6] A. Olaya-Castro, C.F. Lee, F. Fassioli Olsen, and N.F. Johnson, *Phys. Rev. B* **78**, 085115 (2008).
 - [7] P. Rebentrost, M. Mohseni, I. Kassal, S. Lloyd, and A. Aspuru-Guzik, *New J. Phys.* **11**, 033003 (2009).
 - [8] F. Caruso, A.W. Chin, A. Datta, S.F. Huelga, and M.B. Plenio, *Phys. Rev. A* **81**, 062346 (2010).
 - [9] A.W. Chin, A. Datta, F. Caruso, S.F. Huelga, and M.B. Plenio, *New J. Phys.* **12**, 065002 (2010).
 - [10] F. Caruso, S.F. Huelga, and M.B. Plenio, *Phys. Rev. Lett.* **105**, 190501 (2010).
 - [11] C. Brif, R. Chakrabarti, H. Rabitz, *New J. Phys.* **12**, 075008 (2010).
 - [12] M. Shapiro, P. Brumer, *Principles of the Quantum Control of Molecular Processes*, Wiley, New Jersey, 2003.
 - [13] J.L. Herek, *J. Photochem. Photobiol. A: Chem.* **180**, 225 (2006).
 - [14] A.P. Pierce, M.A. Dahleh, H. Rabitz, *Phys. Rev. A* **37**, 4950 (1988).
 - [15] R. Kosloff, S.A. Rice, P. Gaspard, S. Tersigni, D.J. Tannor, *Chem. Phys.* **139**, 201 (1989).
 - [16] S.A. Rice, M. Zhao, *Optical Control of Molecular Dynamics*, Wiley, New York, 2000.
 - [17] V. May, O. Kühn, *Charge and Energy Transfer Dynamics in Molecular Systems*, Wiley, Berlin, 2004 - Chapter 9.
 - [18] J. Petersen, R. Mitric, V. Bonacic-Koutecky, J.-P. Wolf, J. Roslund, and H. Rabitz, *Phys. Rev. Lett.* **105**, 073003 (2010).
 - [19] T. Buckup, T. Lebold, A. Weigel, W. Wohlleben, M. Motzkus, *J. Photochem. Photobiol. A: Chem.* **180**, 314 (2006).
 - [20] J. L. Herek, W. Wohlleben, R. J. Cogdell, D. Zeidler, and M. Motzkus, *Nature* **417**, 533 (2002); J. Savolainen, R. Fanciulli, N. Dijkhuizen, A. L. Moore, J. Hauer, T. Buckup, M. Motzkus, and J. L. Herek, *Proc. Natl. Acad. Sci. USA* **105**, 7641 (2008).
 - [21] B. Brüggemann and V. May, *J. Phys. Chem. B* **108**, 10529 (2004); *Chem. Phys. Lett.* **400**, 573 (2004).
 - [22] P. Doria, T. Calarco, S. Montangero, *Eprint arXiv:1003.3750* (2010).
 - [23] H. Lee, Y.-C. Cheng, G.R. Fleming, *Science* **316**, 1462 (2007).
 - [24] V. I. Prokhorenko *et al.*, *J. Phys. Chem. B* **106**, 9923 (2002).
 - [25] J.M. Olson, *Photosynthesis Research* **80**, 181187 (2004).
 - [26] Jon Marangos, private communication.
 - [27] J. Adolphs and T. Renger, *Biophys. J.* **91**, 2778, (2006).
 - [28] D.E. Tronrud, M.F. Smidt, B.E. Matthews, *J. Mol. Bio* **188**, 443

- (1986).
- [29] R.S Judson, H. Rabitz, *Phys. Rev. Lett.* **68**, 1500 (1992).
- [30] J. Yuen-Zhou, M. Mohseni, and A. Aspuru-Guzik, Eprint arXiv:1006.4866 (2010); P. Reberstrost, S. Shim, J. Yuen-Zhou, and A. Aspuru-Guzik, Eprint arXiv:1012.3451 (2010); J. Yuen-Zhou and A. Aspuru-Guzik, Eprint arXiv:1101.2716 (2011).
- [31] W.H. Press, S.A. Teukolsky, W.T. Vetterling, B. P. Flannery “Numerical Recipes. The Art of Scientific Computing”, Cambridge University Press, New York 2007.
- [32] T. Rowan, “Functional Stability Analysis of Numerical Algorithms”, Ph.D. thesis, Texas Univ. (Austin), 1990.
- [33] S. Montangero, T. Calarco, R. Fazio, *Phys. Rev. Lett.* **99**, 170501 (2007).
- [34] P. Reberstrost, I. Serban, T. Schulte-Herbrüggen, and F.K. Wilhelm, *Phys. Rev. Lett.* **102**, 090401 (2009).
- [35] M.T.W. Milder, B. Brüggemann, v.R. Grondelle, J.L. Herek, *Photosynth. Res.* **194**, 257-274 (2010).
- [36] A. Kaiser and V. May, *Chem. Phys.* **121**, 2528 (2004); *J. Chem. Phys. Lett.* **405**, 339 (2005).
- [37] J.Prior, A.W. Chin, S.F. Huelga and M.B. Plenio, *Phys. Rev. Lett.* **105**, 050404 (2010).
- [38] A.W. Chin, A. Rivas, S.F. Huelga and M.B. Plenio *J. Math. Phys.* **51**, 092109 (2010).
- [39] A. Ishizaki and G.R. Fleming, *J. Chem. Phys.* **130**, 234111 (2009).
- [40] M. Thorwart, J. Eckel, J.H. Reina, P. Nalbach and S. Weiss, *Chem. Phys. Lett.* **478**, 234 (2009).